SAND2019-14503R

Sandia National Laboratories

Final Report

Co-op at Sandia National Laboratories

July - December 2019

Sandia National Laboratories is a multimission laboratory managed and operated by National Technology & Engineering Solutions of Sandia, LLC, a wholly owned subsidiary of Honeywell International Inc., for the U.S. Department of Energy's National Nuclear Security Administration under contract DE-NA0003525.

Mike Winter
Manager, 09435

Jeremy Cummings
Student Intern, 09435

U.S. DEPARTMENT OF ENERGY

National Nuclear Security Administration

Contents

1 Projects

This co-op was performed at Sandia National Laboratories (SNL) within the Weapon Surety Engineering II Department (9435), which is a customer-focused organization that provides engineering and system analysis expertise to ensure a safe deterrent throughout the entire weapon lifecycle. Engineers in 9435 develop a deep knowledge in both component and system function to support rigorous evaluation and mitigation of potential failure modes. They operate across multiple engineering disciplines (mechanical, electrical, computer, materials and systems engineering) with opportunities to develop cross-disciplinary capability. The team supports a variety of stockpile systems and is part of the product teams during development, design and production, as well as advanced concept and exploratory efforts. 9435 engineers use their extensive component and system knowledge, as well as experimental data and modeling, to ensure products function as intended with assured safety. Members of the department learn the function of multiple components, how those components integrate within the system and apply surety principles and processes to ensure a safe, secure, reliable, and effective U.S. nuclear deterrent.

1.1 Magnetic Shielding Research & Testing

Electronic devices are ubiquitous in the modern world, and are susceptible to undesirable effects caused by sources of electromagnetic radiation. These sources range from small components mounted on a circuit board up to high-voltage power generation and transmission equipment and natural events such as lightning.

This project was undertaken to learn about and explore how magnetic coupling to electronic components can be mitigated using special shielding materials designed for that purpose. A thorough literature review was conducted, experts in electromagnetism were consulted, and a report was written which attempted to simplify this very complex topic into a reference document for safety engineers required to perform assessments regarding magnetic shielding. It was written to briefly elucidate how magnetic coupling and shielding works, explain some best practices when designing a shield, and provide information regarding the procurement and manufacture of magnetic shields. A series of experiments was devised to test the shielding effectiveness of two materials, and a proposal was drafted to secure funding and resources to carry them out. The experiments require specialized facilities and technicians to perform, and access was not available before the co-op concluded. The report and experiment protocol were therefore passed on to 9435 management in hopes that the experiments can be integrated in a future project.

Full report on page 4

1.2 Breakdown Voltage Testing

A production run of assemblies designed to provide electrical isolation was discovered to be contaminated with conductive material as a result of an assembly process, and a series of tests was performed to determine the degree to which this could become a problem. The tests involved passing a particular waveform through different configurations of the assembly with varying degrees of contamination; the results of these tests were compiled into a fifteen-page appendix to a larger, more comprehensive report, and forwarded to the appropriate authority so that an informed decision could be made regarding the final disposition of the contaminated assemblies. The contents of the appendix are proprietary and unavailable for release. In lieu of this, a brief summary with simplified graphics is provided.

Appendix summary on page 26

1.3 PMDI Literature Review

Polymethylene Diisocyanate (PMDI)-based rigid polyurethane foam is widely used to encapsulate critical electronic and magnetic components for the purposes of electrical and/or thermal insulation as well as protection from shock and vibration. A literature review was conducted to explore the state of knowledge regarding the mechanical characteristics of these materials, how they react to high-temperature environments, and how homogeneous their cell structure is.

Full literature review on page 28

2 Educational Activities

The following is a list of media content which was reviewed in entirety. These cover a range of topics, including the history of the U.S. nuclear weapons enterprise, past and present theories surrounding nuclear deterrence, geopolitical topics, energy climate, and department-related mechanical and electrical engineering topics.

2.1 Sandia National Laboratories YouTube Channel

"On Deterrence"
"Six Stockpile Modernization Programs"
"U.S. Strategic Nuclear Policy, an Oral History"
"Always/Never: The Quest for Safety, Control, and Survivability"
"Nuclear science" playlist
"Big Science" playlist

2.2 National Security Speaker Series *(not available outside SNL)*

Dr. Paul Scharre: "Autonomous Weapons and the Future of War"
General John Hyten, Commander USSTRATCOM: "A Warfighting Perspective"
General John Hyten, Commander USSTRATCOM: "Preserving our Space and Cyberspace Capabilities"
General Charles Holland: "Military Operations in an Uncertain World"
General O'Neill: "Army S&T Options for the 21st Century"
Lt. General Frank Klotz: "Sustaining the Nuclear Enterprise: Lessons from the Air Force Experience"
Peter Singer: "NextTech: The Future of Technology, Security, and Threats"
Peter Singer: "NextWar: What key trends will shape the new Interwar years?"
Dr. Victor Reis: "Sputnik, Energy, and National Security: A Strategic Planning Perspective"
Dr. Victor Reis: "Strategy, Stockpile Stewardship and the Dangerous Science and Technology Elite"
Dr. Robie Roy: "The National Security AT Enterprise: Challenges and Opportunities"
Dr. Jerry Krill: "Engineering at the Edge of Knowledge"
Ben FitzGerald: "Defense Innovation and the Future of Offset Strategies"
Dr. James Lewis: Cyber Conflict and International Security: Public Goods, Norms, Escalation and Deterrence"
Dr. John P. Holdren: "A Conversation with the President's Science Advisor"
Paul Bracken: "The Second Nuclear Age"
Norman Augustine: "The Foundation of National Security"
Ambassador Ken Brill: "21st Century DOE Lab Complex Is Needed to Deal with 21st Century U.S. National Security Challenges"
General Barry McCaffrey: "Strategic International Security Challenges Facing the United States"
Dr. Gary Samore: "Future of the Prague Agenda"
Dr. Ollo Heinonen: "North Korea, Iran, and Syria – Verification Lessons Learned"
Dr. Siegfried Hecker: "North Korea, Iran, and Syria – What's Next?"
Dr. Gregory Treverton: "A View from the National Intelligence Council"
Secretary Frank Rose: "Future of U.S.-Russia Strategic Stability"
Dr. Bruce Bennett: "Preparing for the Possibility of a North Korean Collapse"
Brad Roberts: "Extended Deterrence and Strategic Stability in Northeast Asia"

Brad Roberts: “Nuclear Posture Review – Background, Results & Implementation”
Richard Samuels: “Japan’s Grand Strategy and Nuclear Weapons Options”
Ambassador Thomas Graham, Jr: “Nuclear Dangers: The Non-Proliferation Treaty under Threat”
Eric Schlosser: “Command and Control”
Dr. Theodore A. Postol: “Why the Ground-Based Missile Defense Will Not Be Reliable in Combat”
General C. Robert Kehler: “The Enduring Role of Nuclear Weapons in U.S. National Security”
Jeff Bingaman: “The Evolution of U.S. Energy Policy”
James Woolsey: “Energy in the 21st Century: Could Muir, Patton and Gandhi Agree on a Program?”
James Clad: “World Politics in a Changing Energy Landscape”
Sarah Chayes: “From Afghanistan to Ukraine: Why Corruption is an International Security Problem”
Dr. Tevi Troy: “Presidents and Disasters”
Dr. Daniel Heimerdinger: “Columbia Accident Investigation Board: An Insider’s Perspective”
Dr. Charles Elachi, Director, JPL: “The Engineering Challenges & Excitement of Robotic Space Exploration”
Sherri Goodman: “Climate Change and National Security: Accelerating Risks, Building Resilience”
Fran Ulmer: “Global Implications of the Rapidly Changing Arctic”

2.3 Required Reading

“Command and Control” by Eric Schlosser
2010 Nuclear Posture Review
2018 Nuclear Posture Review
Department internal technical documents

2.4 Staff Interviews/Meetings/ Department Training

22 interviews with department staff members covering their areas of expertise, experience at SNL, and current projects.
11 Project review meetings
7 Department-level coordination meetings
4 Department technical training sessions

2.5 Other Training & Events

Coordinated and attended a tour for 10 people covering 4 research reactor facilities
Volunteered as a participant in an active shooter training evolution for SNL’s Protective Force
7 live training sessions and 26 online topical trainings; 33 hours total
Began coordinating senior project partnership between OIT, SNL
Attended:
- NASA presentation about planetary defense from near-Earth objects
- Director’s talk concerning the future of SNL
- Internal SNL job fair
- 5 intern project presentations

3 Magnetic Shielding Research & Testing

Magnetic Shielding With Ferromagnetic Materials

Jeremy T Cummings, 09435
November 2019

Introduction

Lightning strikes pose a significant hazard to electronics, particularly within aircraft. This report characterizes the effects of lightning on magnetic circuit elements and the mechanisms by which these effects occur, and offers information on mitigation efforts that might be undertaken through magnetic shielding.

A brief summary of the concepts behind magnetic induction and the characteristics of lightning strikes is followed by an overview of magnetic shielding best practices. Several options for shielding a space or individual component are presented, as well as information regarding simulations for magnetic effects. Finally, a series of experiments were designed to measure the shielding effectiveness of two materials, and to determine to what extent a particular magnetic shield configuration can reduce magnetic coupling in a transformer.

Electricity and Magnetic Fields

Electricity and magnetism are inextricably linked; the following is a brief overview of the mathematical relationships between the two which will be used to inform subsequent sections.

Magnetic Fields and Current

Current moving through a conductor generates a magnetic field around the conductor (Figure 1).

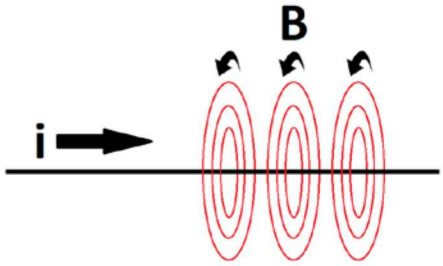

Figure 1: Current traveling through a wire generates a magnetic field

The magnitude of the magnetic field is described by the following equation:

$$\left[B = \frac{\mu_0 i}{2\pi r}\right] \quad \text{Eq. (1)}$$

where: μ_0 = permeability of free space ($4\pi \times 10^{-7}$ H/m)
i = current through the conductor
r = radial distance from the conductor.

From this equation it is clear that: $B \propto I$

$B \propto \frac{1}{r}$

B is in Teslas; 1Tesla = 10000 Gauss

Magnetic Induction

Current moving through a conductor generates a magnetic field as shown above, and the reverse is also true; a magnetic field moving through or changing magnitude in an area enclosed by a conductor loop will generate a current through the conductor.

A magnetic field may be imagined at any given point as a series of parallel lines radiating from a current source. The amount of magnetic field lines passing through a given area is equal to the dot product of the magnetic field vector and the differential area- a quantity known as the magnetic flux, denoted here as φ_B. In other words, the magnetic flux is the amount of magnetic field passing through the projection of an area onto a plane orthogonal to the incident magnetic field lines.

Mathematically:
$[\varphi_B = \int B \cdot da]$ Eq. (2)
Magnetic Induction

From which it is clear that the orientation of the current channel generating a magnetic field with respect to the area in question is of considerable importance; see Figure 2.

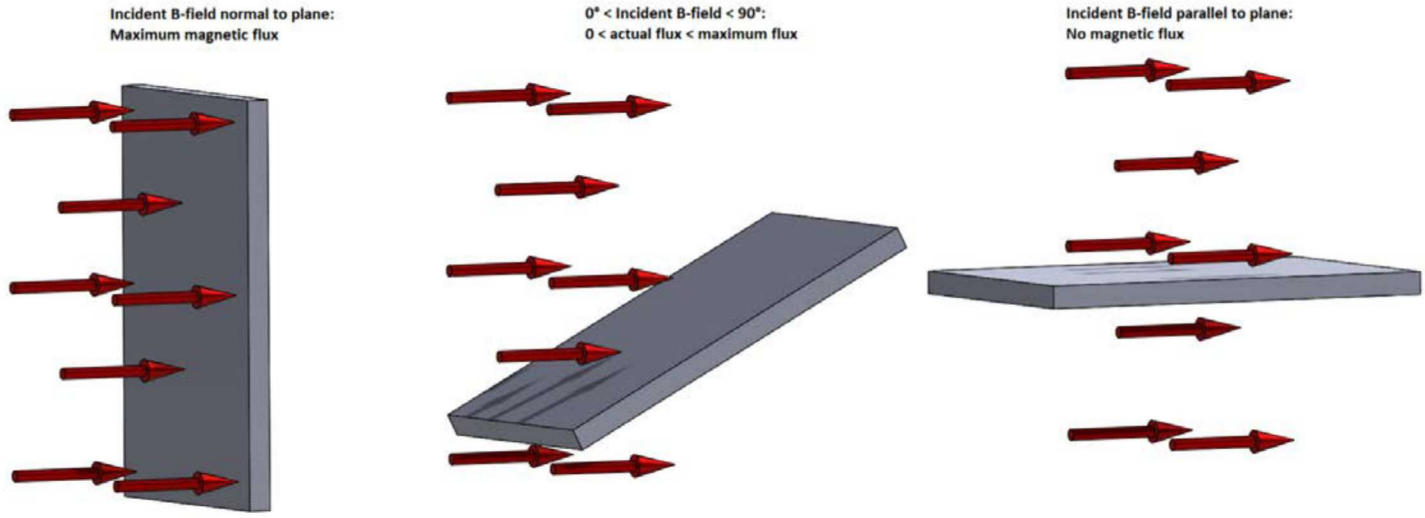

Figure 2: Magnetic flux through a plane depends on the incident angle of the magnetic field relative to a plane.

If the area of interest is known, the magnetic flux φ_B can be expressed as:

$[\varphi_B = BA\ Cos\ \theta]$ Eq. (3) where: A = area of interest
θ = angle between a vector normal to the plane and the incident magnetic field

A voltage will be induced in a conductor loop if the area enclosed by the loop is present in a *changing* magnetic field – that is, if the magnitude changes or the magnetic field moves relative to the loop – a relationship described by the following:

$[V = -\varphi_B\ dt\ ]\ \therefore\ \left[V = -\int_0^{dt} B \cdot ds\right]$ Eq. (4)

Lightning and Skin Depth

The *skin depth* of a current channel, which is a measure of how deep into the surface of a material current will flow, is defined as follows:

$\left[\delta = \sqrt{\frac{\rho}{\omega\mu}}\right]\ \therefore\ \left[\delta = \sqrt{\frac{\rho}{\pi f \mu}}\right]$ Eq. (5) where: μ = relative magnetic permeability of the conductor
ρ = resistivity of conductor material

This is important when considering higher-frequency signals, and will be treated further below.

Lightning Strikes

Lightning is a broad-frequency, high-current pulse of electricity. The electromagnetic frequency range of lightning is about 1 Hz to 300 MHz, with a peak in the area between 5 kHz – 10 kHz, and the current can be as high as 200 kA. This generates an extremely strong, changing magnetic field, which could induce a magnetomotive force (voltage) in electrical components and cause unwanted events to occur in critical circuitry.

Aircraft fuselages are made from aluminum, which has a high electrical conductivity that almost guarantees a lightning current channel will run along the surface of the fuselage and not penetrate through the aircraft's skin (Eq. 5). Industry is researching composite materials as a replacement for aluminum structural components like the fuselage, but the composites developed so far offer no such protection. Lightning normally attaches to an aircraft near the nose, passes along the fuselage in a narrow channel, and discharges out the aft end, and any electronics located in close proximity to the skin could be affected. If current were to penetrate through a composite fuselage, the high current itself would become a significant threat in addition to magnetic effects, and provisions would have to be made to shield electrical components within the aircraft so that a penetrating current channel would behave in the same way as if it struck an aluminum fuselage- for example, a streamlined aluminum capsule within the aircraft that contains critical circuitry. The typical forward-to-aft current channel is very similar to the situation illustrated in Figure 1, which will thus be used as the model for a lightning strike in this report.

Although lightning has a broad range of constituent frequencies, most of the higher frequencies are attenuated in the aluminum surface of an aircraft via eddy currents (Eq. 5) like radio-frequency signals, while the lower frequencies penetrate deeper and pose a greater risk of magnetic coupling. Lightning is also a very short-duration event; the threat can therefore be simplified for modeling and experiment by treating it as a single cycle of a large-amplitude direct current square wave with a rapid rise time.

Mitigation Options

There are several parameters that affect the amount of voltage a magnetic field may induce in a circuit, per the previous expressions. Referring to Eq. (1), the distance between a current source and electronics should be maximized to reduce magnetic flux density; the magnetic field strength drops as the square of the distance from the current channel. Depending on the size, location, and configuration of a component or system, physical constraints could severely limit the extent to which this principle may be exploited.

Reducing the area through which magnetic fields may travel is another method of reducing magnetic coupling, and could be accomplished in two ways:

1) Orienting all circuit loops such that they are parallel to the incoming magnetic field
2) Minimizing the cross-sectional area of circuit loops.

Option 1) is not a practicable means of mitigation, as it is not possible to plan for the orientation of a current channel due to a lightning strike; however, the orientation of magnetic circuit devices could be adjusted to minimize coupling based on the most likely configuration of the current channel- forward to aft in an aircraft.

Option 2) is already a standard practice in circuit design when it comes to the placement of traces on a circuit board; a loop on a printed circuit board functions as an antenna, and circuit designers must ensure that individual conductor loops don't interfere with one another (crosstalk) or have enough area for considerable current to be induced. However, of greater concern are magnetic circuit components like inductors or solenoids, as the function of these components relies on magnetic induction; the extent to which the loop area can be minimized while retaining component function is limited.

In short, it is inevitable that magnetic fields of some magnitude will be present within an aircraft during a lightning strike. Because the exact orientation of circuit components relative to these magnetic fields is unknowable, and certain components rely on magnetic coupling for their normal function, the most effective option to mitigate the effects of unwanted magnetic coupling is the use of a magnetic shield tailored specifically for this purpose.

Magnetic "Shielding"

In the interests of both brevity and clarity, a mathematical representation of magnetic shielding will be eschewed here in favor of a graphical explanation. Magnetic shielding expressions comprise several layers of mathematical operations – rigorous treatments fill entire chapters or books and draw upon dozens of concepts from physics, an effort which will not be repeated here – but some simple guidelines may be derived from them. Furthermore, magnetic shield design benefits from decades of industry experience which support these guidelines, and a reputable vendor could assist with shield design given a few parameters. A brief summary of magnetic shielding principles follows, as well as a list of best practices when designing a magnetic shield. For a more detailed explanation, the reader is encouraged to consult Celozzi and Rikitake, with the author's compliments*.

Magnetic shields don't actually *block* magnetic fields – nothing will stop the field lines from completing a loop – but rather provide a "path of least resistance" for the fields to travel through. The material property that quantifies this tendency is a material's relative permeability (μ), which is a ratio of a material's permeability relative to the permeability of free space (μ_0). The higher this ratio, the more a magnetic field will be diverted through the material of a magnetic shield. This effect can be likened to electrical conductivity; as more current will flow through a material with higher conductivity than one with lower conductivity, more magnetic field will flow through an area with higher permittivity. In a cylindrical ferromagnetic shield with high relative permeability, the lines of flux are drawn into the material almost perpendicular to the shield surface and then shunted along the shield almost parallel to the surface, as shown in Figure 3. Some magnetic field penetrates, but the flux is lower than outside the shield.

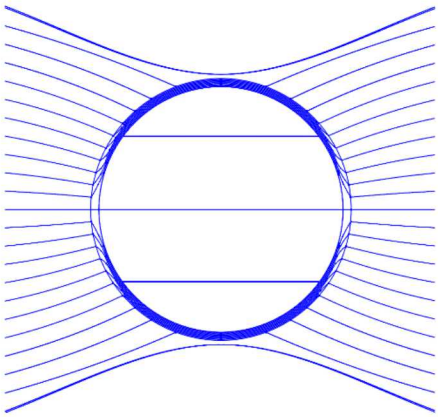

Figure 3: Magnetic field distribution for cylindrical ferromagnetic shield subjected to a uniform field

Saturation induction is a measure of how much flux a material can shunt along its surface in this way; once a material is magnetically saturated, it cannot shunt any more flux, and any flux above the saturation point of the material will simply pass through. The relationship between the magnetic field strength and the flux through a material is described by the material's B-H curve. High-saturation materials are good for shielding strong magnetic fields, but generally have lower permeability, while high-permeability materials generally have a lower saturation point. High-saturation materials are best used as the outer layer in a multi-layer shield design; the outer shield drastically reduces the magnitude of the magnetic field by attenuation, and the inner, high-permeability shield(s) can effectively shunt what penetrates through the outer shield. At the edges of a planar shield or the ends of a cylindrical shield, unpredictable "edge effects" occur; this is similar to what would happen at these points if the shield were stationary in a moving fluid. Accordingly, a shield should extend beyond the component of interest to such a degree that edge effects are inconsequential. A quick heuristic for cylindrical shields is that the shield should extend beyond the shielded component a distance equal to the shield diameter on either side.

* Be forewarned, Celozzi, an electrical engineering professor with 3 decades of experience, author of dozens of publications including the textbook on electromagnetic shielding to which the reader is referred, describes the theoretical analysis of low-frequency magnetic field shielding as "very trying to carry out."

Magnetic "Shielding"

There are several factors that influence the effectiveness of a shield in decreasing magnetic flux:

- Material (intrinsic properties such as μ and σ)
- Shape
- Wall thickness, layers, and spacing

Materials

Several materials are commonly used for magnetic shielding. For high-frequency shielding, materials with high electrical conductivity (σ) such as aluminum or copper are appropriate, as eddy currents induced by the oscillations effectively cancel one another out. For lower-frequency signals and transient events like lightning, iron-nickel or iron-cobalt alloys are the most common.

Among iron-nickel alloys, a higher percentage of iron corresponds to a higher saturation point and lower permeability at a given field strength compared to an alloy with lower iron content; 99.99% Fe is available, and offers good shielding characteristics at high field strengths due to its high saturation point. On the opposite end of this spectrum, permalloy, MuMetal® HyMu 80®, and other alloys referred to colloquially as "mu-metals" are usually about 80% nickel, 20% iron with small amounts of molybdenum and traces of other elements; they offer higher permeability at a given field strength vs. high-purity iron, but with a correspondingly low saturation point.

Iron-Cobalt alloys such as Hiperco® 50 offer even higher saturation points than high-purity iron (about 10% greater), as well as higher initial and maximum permeability- but these benefits come at a significantly higher cost; Hiperco® 50 is 48.75% cobalt, 1.9% vanadium, and 0.05% niobium, all of which are rare and expensive elements. Hiperco® alloys are most commonly used in motors and generators that require a high field strength-to-weight ratio (airplane auxiliary generators and motors), but their relatively high permeability at high field strengths could make them a good candidate for shielding material where spatial considerations preclude multi-layer shields.

Shape

For an in-depth explanation of how shield geometry affects shielding effectiveness, see T. Rikitake, chapter 2. Simply put, a spherical shield is ideal because it almost eliminates edge effects; a cylindrical shield is the next-best option, and rectangular shields with flat shielding surfaces are the least effective. In any event, predicting shield effectiveness for a given configuration requires simulation software designed to solve such a problem, vast computing resources, and a considerable amount of time.

Wall thickness

For oscillating signals, shielding is effected by the cancellation effect of eddy currents. Skin depth is inversely proportional to frequency; if a shield were the same thickness as the skin depth of an incident signal (thin for a high-frequency signal), the signal would flow uniformly over the shield thickness and the shield would not be very effective; however, if the thickness of the shield is much greater than the skin depth of a signal, eddy currents induced in the shield cancel out much of the signal and thereby offer good shielding effectiveness.

With low-frequency signals, however, the shielding mechanism is flux shunting. This deflection of flux flowing through the material of a shield is most pronounced on the inner surface of the shield, so although a thinner shield will have less mass and therefore reach its saturation point faster, the flux will also be deflected sooner than would be the case with a thick shield. This means that with a given radius, several thin concentric shields are more effective than a single thick shield, especially if space is left between them. For both spherical and cylindrical shields, Rikitake notes a drastic increase in shielding effectiveness by simply using two physically separated thin shields in place of a single thick shield. This approach offers the added benefit of reducing the requisite mass of shielding material, thereby reducing cost and weight.

Numerical Modeling

It is reasonable to expect that computer simulation would be appropriate for such mathematically complex problems as magnetic shielding, and that may in fact be the case; unfortunately, the learning curve for the software was steep enough that the author chose to pursue an experimental route due to time constraints. Furthermore, Celozzi warns that due to the complexity of the computations, using commercial numerical modeling software for such an application may result in inaccurate results unless the software was specifically designed for it; this particular problem may require purpose-built numerical modeling in both the frequency and time domains (see Celozzi, Ch. 5 and pages 286-287).

Simulations of this general type have been conducted in ANSYS Maxwell 2D and COMSOL by experienced users in 9432, but unexplained effects and technical difficulties have arisen. (As an aside, Dassault Systèmes' CST suite has been used elsewhere for lightning simulations and may prove useful.) Even when additional parallel computing resources were applied to these problems, a single solution could take up to 7 hours- and still be inconsistent with reasonable expectations and empirical results, requiring more troubleshooting. An effort towards conducting numerical modeling of this problem would benefit from the involvement of a specialist in numerical modeling.

Mechanical Attributes of Magnetic Shielding Materials

High-purity iron is ductile and has a Young's modulus of 211GPa. It is machinable, but requires that certain provisions be taken due to its ductility. Whether it is hardenable and via what methods is unknown, nor is information regarding the corrosion susceptibility of pure iron or its weldability. These would be fertile areas for experimentation- particularly tests examining galvanic corrosion with a range of dissimilar materials, intergranular corrosion after welding, weldability, and hardenability via heat treatment and cold working.

μ-metal is ductile and has a Young's modulus of 217GPa.It is similar to 300-series stainless steels in several respects: it offers good corrosion resistance due to its high nickel content, and is challenging to machine for the same reason, tending to be "gummy". μ-metal is readily welded with traditional processes. It is hardenable through cold working, but not through heat treatment- and in fact must undergo a specialized annealing process in a dry hydrogen atmosphere to maximize its permeability following any forming or machining process. This latter requirement may make μ-metal undesirable for structural components.

Shield Configurations

Planar Shield

Advantages:

- Small footprint and low height for surface-mount applications
- Easy to manufacture (hydroforming, pressing)
- Available commercially
- Custom work would be relatively inexpensive due to manufacturing process

Disadvantages:

- COTS products generally small, thin, limited materials available
- Planar shields generally offer inferior shielding vs. cylindrical, spherical shields

Shield Configurations

Cylindrical Shield

Advantages:

- Better performance than planar shield
- Easy to manufacture (deep drawing/pressing/hydroforming)
- Vertical mounting options commercially available

Disadvantages:

- Larger footprint and height; more wasted space for surface component
- Transverse mounting for surface components not commercially available
- Novel attachment method required for transverse surface mount application

Spherical Shield

Advantages:

- Best possible configuration; offers same shielding effectiveness from all directions
- Thin shields could be inexpensively custom-made

Disadvantages:

- Manufacture of thicker shields could be expensive (require machining)
- Novel attachment method required
- Larger footprint and height; more wasted space for surface component

Shield Sourcing Options

Magnetic Shield Corporation

Located in Bensenville, Illinois. Offers custom shield design, hydrogen annealing, and a multitude of forming, cutting, welding, and finishing processes. Three materials in multiple thicknesses and pre-formed shapes available. This company has been in operation for 75 years and provides the most comprehensive range of services available for the manufacture of magnetic shielding solutions. Price quotes are available upon request.

MuShield

Located in Manchester, New Hampshire. Custom shield design, laser welding, and hydrogen annealing. Two materials in multiple thicknesses available. Price quote for notional parts in Table 1; all shields are single-layer, 0.040" thick, with custom-formed hemispherical end caps- one laser-welded on, one slip-on. Price includes hydrogen annealing. Batch deliveries could begin six weeks after order receipt.

Table 1: MuShield Price Range

	Cost/unit, delivered	
Shape	80% Ni, 20% Fe	49% Ni, 51% Fe
12" OD X 8" Cylinder	$475	$375
5" OD X 8" Cylinder	$160	$125
1" OD X 1.5" Cylinder	$35	$32
0.5" OD X 1.5" Cylinder	$33	$32

Shield Sourcing Options

Ad-Vance Magnetics, Inc.

Located in Rochester, Indiana. Custom shield design and hydrogen annealing. Three materials in multiple thicknesses available. Price quote for notional parts in Table 2; all shields are single-layer, 0.040" thick, with custom-formed hemispherical end caps, both slip-on. Price includes hydrogen annealing. Lead time for such an order would be approximately eight weeks.

Table 2: Ad-Vance Magnetics Price Range

Shape	Cost/unit, delivered		
	80% Ni, 20% Fe	48% Ni, 52% Fe	High-purity Fe
12" OD X 8" Cylinder	$440	$340	$125
5" OD X 8" Cylinder	$154	$120	$64
1" OD X 1.5" Cylinder	$32	$31	$33
0.5" OD X 1.5" Cylinder	$23	$22	$24

Amuneal

Located in Philadelphia, Pennsylvania. Custom shield design, laser welding, and hydrogen annealing. One material available in multiple thicknesses. Price quote for notional parts in Table 3; all shields are single-layer, 0.040" thick Amumetal (80% Nickel, 20% Iron), custom-formed hemispherical end caps- one end laser-welded on, one slip-on. Price includes hydrogen annealing. Such an order would have an approximate five-week lead time.

Table 3: Amuneal Price Range

Shape	Cost/unit, delivered
12" OD X 8" Cylinder	$1,410
5" OD X 8" Cylinder	$705
1" OD X 1.5" Cylinder	$470
0.5" OD X 1.5" Cylinder	$460

Information Resources

This paper barely scratches the surface of the phenomenon of electromagnetism; for more expansive and detailed information, the reader is encouraged to refer to Tables 4-6 as a jump-off point for further research.

Table 4: Topical Books

Books				
Title	Author	Year	Recommended Sections	Notes
"Fundamentals of Electricity and Magnetism"	Kip, A.	1969	All	Hardcopy available at Tech Library
"Electromagnetic Fields and Energy"	Haus, H.	1989	Chapters 1, 2, 3, 5, 8, 10	Soft copy available at ocw.mit.edu
"Magnetic and Electromagnetic Shielding"	Rikitake, T.	1987	Chapter 2, Pages 5-107, particularly graphics	Hardcopy available for loan through Tech Library
"Electromagnetic Shielding"	Celozzi, S. et al.	2008	Appendix B, Pages 282 - 314 Materials, Page 21 Thin Films, Page 30 Polymers, Page 32 Special Materials, Page 33 Shielding Effectiveness, Page 43 Multiple Shields, Page 66 Numerical Methods, Page 87 Calculation Methods, Page 286	Soft copy available through Tech Library (Ebook Central)
"Optical Magnetometry"	Budker, D. et al.	2013	Chapter 12: Magnetic Shielding	Soft copy available through Tech Library (Ebook Central)

Table 5: Topical Journals

Journals				
Title	Author	Year	Recommended Sections	Link
The Bell System Technical Journal, Vol. XVII	Various	1938	Pages 417 - 437	http://tiny.sandia.gov/zrlvw
Electromagnetic Methods of Lightning Detection	Rakov, V.	2013		http://tiny.sandia.gov/rskcd
New Dimensions in Shielding	Cowdell, R.	1968		http://tiny.sandia.gov/udc95
Combined use of Magnetic and Electrically Conductive Fillers in a Polymer Matrix for Electromagnetic Interference Shielding	Wu, J & Chung, D.	2008		http://tiny.sandia.gov/hivcn
Analysis of Shielding Effectiveness in the Electric Field and Magnetic Field and Plane Wave for Infinite Sheet Metals	Loya, S.	2016		http://tiny.sandia.gov/kift0
Calculation of an optimized design of magnetic shields with integrated demagnetization coils	Sun, Z et. al	2016		http://tiny.sandia.gov/8ek3s
Overview of Radiation Hardening Techniques for IC Design	Yu, F. et. al	2010		http://tiny.sandia.gov/09e78
Magnetic diffusion and the motion of field lines	Wilmot-Smith, A. et. al	2005		http://tiny.sandia.gov/tl9sp
Electromagnetic Interference Shielding Polymers and Nanocomposites - A Review	Jiang, D et. al	2019		Search in Ebook Central
The power, energy, momentum and the action of the electromagnetic radiation fields of lightning return strokes	Cooray, V	2018		http://tiny.sandia.gov/nf73q
The physics of fast Z pinches	Ryutov, D et. al	1999		http://tiny.sandia.gov/im65v

Information Resources

Table 6: Helpful Links

Links		
URL	Description	Notes
http://tiny.sandia.gov/5fqkv	MIT textbook on EM	Navigate using buttons on page. Change chapters by modifying number after "navigate" in URL, for example, http://web.mit.edu/6.013_book/www/navigate10 opens chapter ten for navigation with buttons.
http://tiny.sandia.gov/puzso	Various info on shielding	
http://tiny.sandia.gov/kwbo1	Low-frequency magnetic shielding	
http://tiny.sandia.gov/gjsf3	Surface-mount shielding options	
http://tiny.sandia.gov/mbxpi	Catalog for board-level shields	
https://hollandshielding.com/	Various shielding products	
http://tiny.sandia.gov/eyjat	Mu-Metal info brochure	Contains B/H curves for high-permeability material, ~80% /20% Ni/Fe
http://tiny.sandia.gov/pxuk2	Co-Netic info brochure	Contains B/H curves for intermediate magnetic shielding material
http://tiny.sandia.gov/y45xw	Netic info brochure	Contains B/H curves for high-saturation magnetic shielding material
http://tiny.sandia.gov/xj9n7	Small optical magnetometer concept	
http://tiny.sandia.gov/wr76u	Small, sensitive magnetometer	
http://tiny.sandia.gov/xjas9	CST simulation software brochure	
http://tiny.sandia.gov/j5e3a	Characteristics of lightning current	

Notional Shielding Experiments

Planar Shield

A planar shield similar to the setup in Figure 4 (see appendix A for complete experiment protocol) offers the least expensive option for validating a simulation, assuming 1) the experiment is conducted in an anechoic chamber or the fixture is placed upon material that attenuates electromagnetic radiation so as to reduce coupling from fields wrapping around the outside of the shield and 2) the simulation is set up to accurately reflect the physical phenomena.

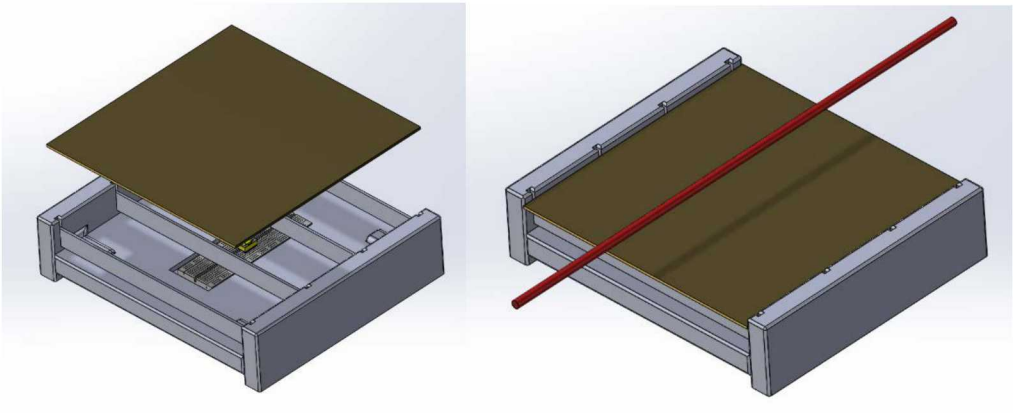

Figure 4: Planar shield experiment setup

Cylindrical Shield

A cylindrical shield offers better protection than a flat shield, as one need only be concerned about magnetic edge effects at the ends of the cylinder. A three-layer, cylindrical μ-metal shield is proposed for use the in experiment in appendix A, similar to the one shown in Figure 5; several sizes of these shields are available commercially in an annealed condition to maximize magnetic permeability. Three layers of 0.025”-thick μ-metal shields are separated by ABS spacers; one end of each shield is welded on while and the other end has a slip-on cap, and the slip-on ends have small penetrations for leads.

Figure 5: Cylindrical shield

Spherical Shield

A spherical shield would offer the best shielding effects, particularly if the shield were comprised of several layers. Figure 6 shows a possible experiment setup. The base is additively-manufactured from ABS plastic, and holds the lower half of a two-piece outer sphere of either high-purity magnetic iron or Hiperco50® iron-cobalt alloy with a diameter of about 2.5 inches. An ABS sphere with a thickness of about 0.25 inches rests within the outer sphere and acts as a spacer between the two magnetic shields; an inner sphere of μ-metal (~80% Nickel, 20% Iron) rests within this spacer. A small, surface-mount transformer is mounted on a piece of perforated circuit board that is cut to fit snugly inside the inner sphere. Leads to and from the transformer pins exit the central sphere via round holes which are aligned with cutouts in the perf-board. Cutouts in the ABS spacer sphere leave room for the leads to exit through holes in the outer sphere, which are offset by 90° with respect to the holes in the inner sphere to minimize edge effects around the penetrations. Alternatively to using a single, thick μ-metal inner shield, an assembly of several thin shield layers and spacers with the same inner and outer dimensions could be used to see if an increase in shielding effectiveness could be realized.

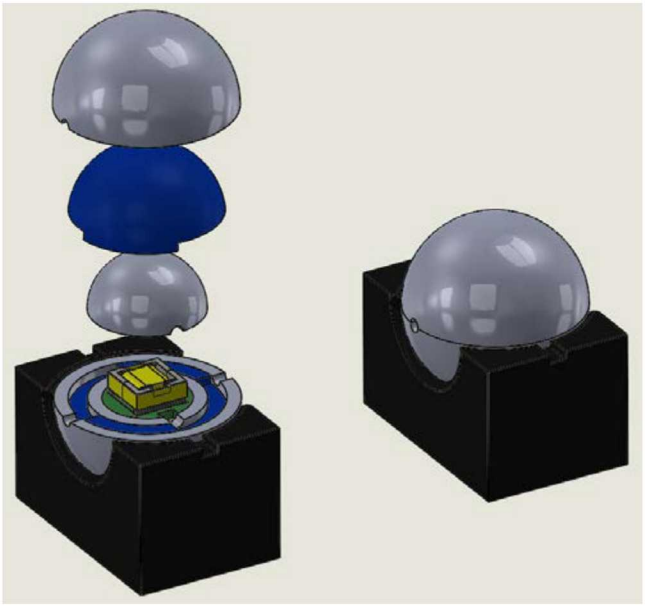

Figure 6: Proposed magnetic shielding test fixture

This type of shield has some significant disadvantages in terms of practical use and production. It would be expensive to manufacture, particularly if the shields are thick, and it would occupy much more space within an enclosure relative to the size of the component it is protecting. Regarding the inner shield, thin μ-metal sheets could easily be hydroformed or drawn into a hemisphere- but a thicker shell would have to be machined from bar stock. High-nickel alloys tend to be “gummy” and easily gall, and machining a hollow hemisphere to a certain tolerance is a lengthy, expensive process. After machining, a μ-metal shield would have to undergo a special annealing process to maximize permeability. In addition to the time spent machining the inner shield, machining from bar stock would involve a great deal of material waste. The outer shield would also have to be machined above a certain thickness; magnetic iron machines reasonably well, but Hiperco50® is gummy like μ-metal and very expensive owing to its cobalt content.

Appendix A: Planar & Cylindrical Shielding Experiment to Mitigate Magnetic Coupling

Summary

Two experiments to test how effective different materials are at mitigating magnetic coupling to electrical components.

Experiment 1: Measure the shielding effectiveness of a 99.99% pure iron plate, a plate of μ-metal (80% Ni/20% Fe), and a multi-layer cylindrical shield of μ-metal.

Experiment 2: Determine whether and to what voltage a transformer in close proximity to high current will charge a capacitor through magnetic coupling, and how effective the materials tested in experiment 1 are at mitigating this effect.

The fixture, shielding material, components and leads will be procured with 09435 funding. The experiments will require about 16 work hours, and will require a high-current source, signal generators, and a means of measuring magnetic field strength. Hazards include high voltage and the presence of a large capacitor.

Experiment 1: Shielding Effectiveness of Fe, μ-metal

The purpose of this experiment is to measure the reduction in magnetic field strength caused by diffusion through iron-based and nickel-based alloys. A magnetometer is placed in close proximity to a wire through which high current is passed; the magnitude of the magnetic field is measured unshielded, and then two types of metal sheets are placed, one at a time and at several discrete distances from the magnetometer, between the current source and the magnetometer in order to measure if and how much each of these metals reduces the magnetic field magnitude. Figures 1 and 2 show the proposed fixtures, which will be additively manufactured from ABS plastic; each is designed to hold components such as magnetometers or transformers, and the planar setup has vertical spacers in three lengths to offset the distance between the magnetometer and the metal sheet: 0.125", 0.5", and 1". Other distances could be tested as well by printing spacers of appropriate width. Two types of materials – high-purity iron (99.99% Fe) and μ-metal, of any desired thickness – should be tested. The "Zero-Gauss" chamber in the cylindrical setup is comprised of three layers of μ-metal separated by non-conductive spacers.

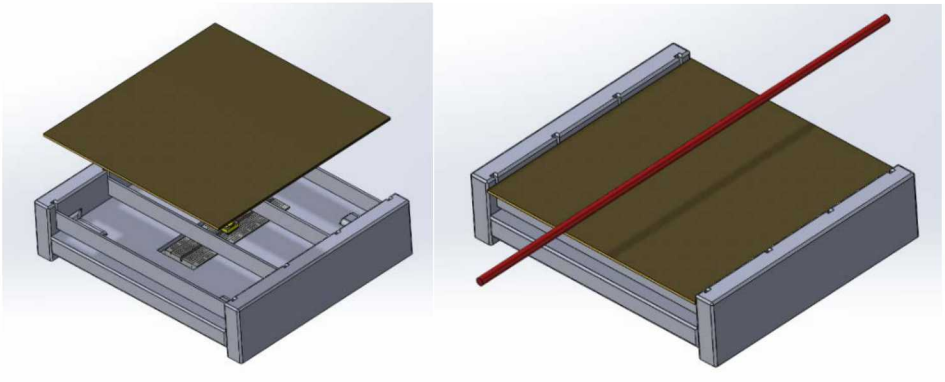

Figure 1: Planar setup for experiments 1 & 2

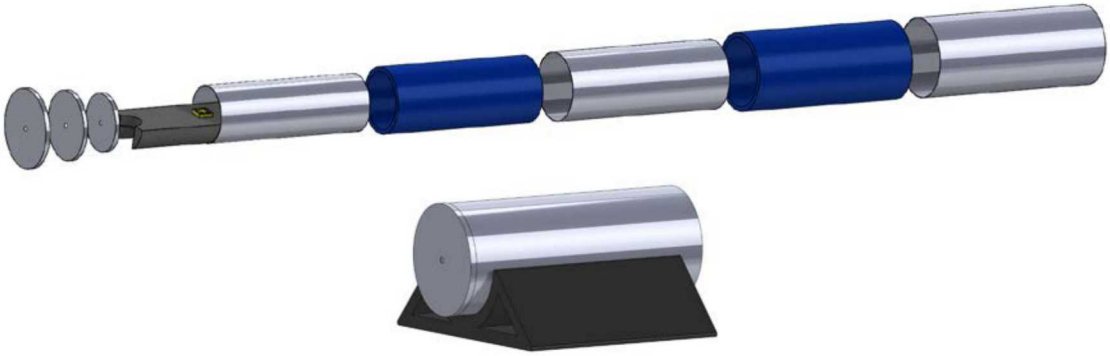

Figure 2: Cylindrical "Zero-Gauss" chamber for experiments 1 & 2

Experiment Outline

A wire will be secured above the fixture, parallel to the metal plate and centered front-to-back with respect to the fixture. The fixture should be placed upon a material that will eliminate reflections of the electromagnetic fields, or the experiment should be conducted within an anechoic chamber designed for such purposes. Leads coming from the magnetometer will be shielded to eliminate error arising from magnetic coupling directly to the leads. Braided, shielded cable designed for low coupling within an additional layer of flexible mu-metal conduit should be used for this purpose.

The data of interest for this experiment is the magnitude of the magnetic field measured at the surface of the fixture; a Hall Effect sensor/Teslameter should be used. The highest current level possible should be passed through the conductor, and the magnetometer used should record/display the maximum magnetic field strength measured. The current should be sent along the conductor in a single, short-duration pulse with a rise time of 10μs and a decay time of 200μs. Thirty shots will be required: three with no shielding, three shots per spacing increment for each of the two shielding materials, and three shots for the "Zero-Gauss" chamber. Assuming a 30-minute setup, five minutes per shot, ten minutes to change spacers and shields, and twenty minutes to set up the "Zero-Gauss" chamber, this experiment should take two people about four hours to complete. An experiment protocol and data collection sheet for this experiment follows.

Experiment 1 Protocol & Checklist

	Action	Initial	Notes
Initial Setup	Connect the magnetometer to the breadboard so that it is centered on both axes, and insert the breadboard into the slot in the base of the fixture that is sized for this purpose.		
	Solder a single set of leads that will remain secured in a breadboard to the ends of the braided wire. Sheathe the wires within the flexible conduit; attach the other end of the leads to the appropriate measurement instrumentation.		
	Place the fixture atop E-field absorber, centered under the conductor so that the long axis of the breadboard is aligned with and parallel to the conductor. If the test is performed in an anechoic chamber that prevents reflections of EM energy, disregard this step.		
	Adjust conductor so that it is 3" above the top surface of the magnetometer and parallel to the bottom surface of the fixture. Measure and record the actual height.		
	Secure the soldered leads to the holes on the breadboard adjacent to the holes occupied by the magnetometer pins.		
	Set up the current source and signal generator; record the current magnitude, voltage, and signal rise time. The target rise time is 10 µs with a decay of 200 µs.		
Unshielded	Ensure that all data is recorded on the attached data sheet for experiment 1.		
	Conduct a total of three shots and record the magnetic field strength for each: Discharge a single square-wave of current through the conductor; measure and record the strength of the magnetic field in Teslas or Gauss and note the units used.		
High-purity Fe	Place one 0.125" spacer in each of the four vertical slots on either side of the fixture, and carefully place the high-purity iron plate on the top of the spacers, ensuring adequate space between the top of the magnetometer and the bottom of the plate.		
	Conduct three shots using the same current and signal characteristics as previous; record the magnetic field strength for each shot on the datasheet.		
	Remove the plate, replace the 0.125" spacers with the 0.5" spacers, and perform 3 shots. Record each shot.		
	Remove the plate, replace the 0.5" spacers with the 1" spacers, and perform 3 shots. Record each shot.		
µ-metal	Place one 0.125" spacer in each of the four vertical slots on either side of the fixture, and carefully place the µ-metal plate on the top of the spacers, ensuring adequate space between the top of the magnetometer and the bottom of the plate.		
	Conduct three shots using the same current and signal characteristics as previous; record the magnetic field strength for each shot on the datasheet.		
	Remove the plate, replace the 0.125" spacers with the 0.5" spacers, and perform 3 shots. Record each shot.		
	Remove the plate, replace the 0.5" spacers with the 1" spacers, and perform 3 shots. Record each shot.		
Zero-Gauss Chamber	Remove the magnetometer and leads from the breadboard and solder the leads directly to the pins of the magnetometer. Place the magnetometer in the fixture, thread the leads through, and assemble the chamber. Slide the conduit up to the opening of the chamber so that it covers as much of the leads as possible. Place the chamber in the cradle, and adjust the conductor so that it is 3" above the center of the chamber.		
	Center the fixture under the conductor, aligned axially.		
	Perform three shots and record each shot on the datasheet.		

Date of Test:

Experiment 1: Shielding Effectiveness of Fe, μ-metal, planar shielding fixture and Zero-Gauss chamber

Current: Voltage: Rise Time: Conductor Height:	Magnetic Field Strength											
	Unshielded			High-Purity Iron			MuMetal			Zero-Gauss Chamber		
	Shot 1	Shot 2	Shot 3	Shot 1	Shot 2	Shot 3	Shot 1	Shot 2	Shot 3	Shot 1	Shot 2	Shot 3
Spacing 0.125"												
0.5"												
1"												
	Mean									Mean		
Mean 0.125"												
Mean 0.5"												
Mean 1"												
0.125" Spacing												
Reduction, Tesla												
Reduction %												
Shielding Effectiveness												
0.5" Spacing												
Reduction, Tesla												
Reduction %												
Shielding Effectiveness												
1" Spacing												
Reduction, Tesla												
Reduction %												
Shielding Effectiveness												
	Comments/Observations			Comments/Observations			Comments/Observations			Comments/Observations		

Test Engineer

Date

Facility Engineer

Date

Safety Engineer

Date

Manager Consent-to-Test

Date

Experiment 2: Magnetic Coupling in a Transformer

The purpose of this experiment is to determine if, and quantify to what degree, a capacitor will be charged when connected to a surface-mount transformer in the presence of a strong magnetic field, and to determine how effectively the shielding materials tested in Experiment 1 will mitigate this unwanted magnetic coupling. The experiment setup will utilize the same fixtures used in Experiment 1, but a small, surface-mount transformer will be used in place of a magnetometer. The transformer will be part of a circuit as illustrated in Figure 3.

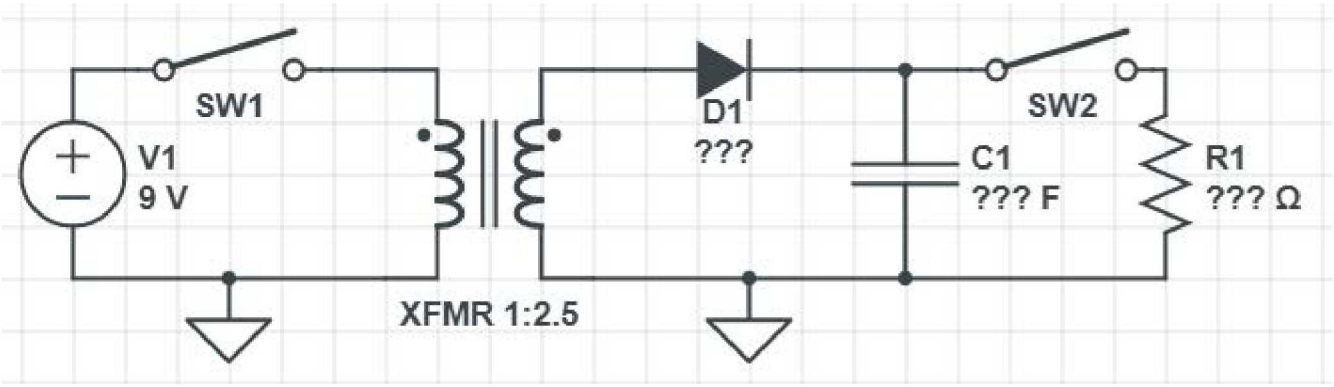

Figure 3: Circuit configuration for experiment 2

This is essentially a capacitive discharge unit (CDU), which is commonly used in gas turbine engine ignition systems and to drive solenoids. An oscillating current through the primary (left) coil of the transformer generates a magnetic field that couples to and is amplified by the secondary (right) coil. During the rise and fall of the input signal, the change in the primary coil's magnetic field induces a voltage across the secondary coil, which sends current through the diode and charges the capacitor. The resistor is present to provide a safe, passive discharge mode for the capacitor. The motivation for this experiment is that a nearby lightning strike could cause sufficient magnetic coupling to induce a current that charges the capacitor and results in an unsafe circuit condition.

The transformer used for this experiment is a Würth Elektronik model 750315252, shown in Figure 4. The primary-side windings are insulated, and comprise 21 loops wrapped around the secondary windings. The secondary windings are laquered, double-strand, and physically wrap the spool 27 times for a total loop count of 54. This results in a winding ratio of about 2.5. To simplify simulation and analysis using a cylindrical model, the following coil dimensions are provided:

(Measurements in Inches)	OD	ID	Wire Thickness	Wire Material	Notes	Length	Eq. Cylinder Thickness
Outer (Primary) Windings	0.380	0.295	0.016	red copper	Laquered	0.536	0.085
Inner (Secondary) Windings	0.295	0.200	0.018	???	Insulated	0.536	0.095

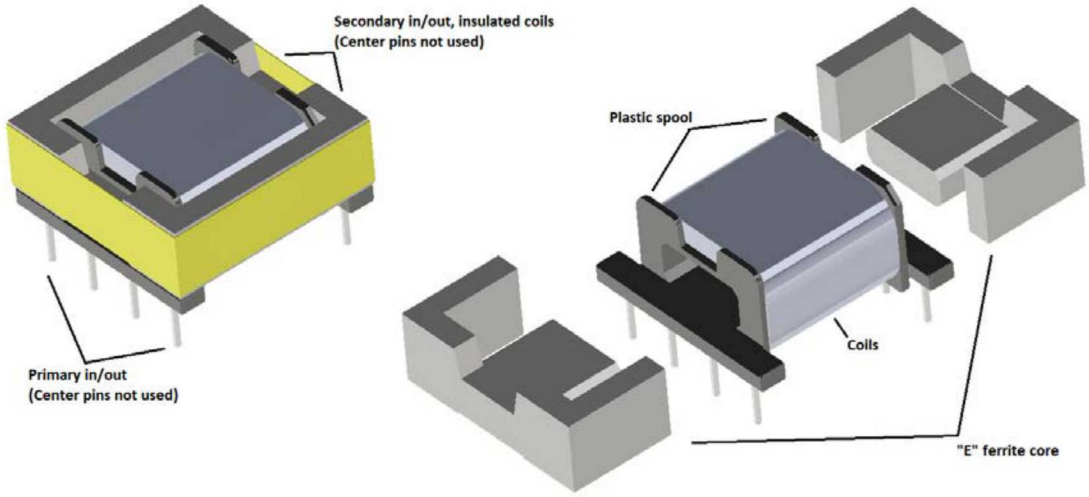

Figure 4: Würth Elektronik model 750315252 transformer

Experiment Outline

The data of interest for this experiment is the voltage induced across the capacitor. First, the function of the CDU circuit must be tested; this may be accomplished by setting up a multimeter to measure the DC voltage across the capacitor, then subjecting the primary side of the transformer to a 5V, 100 kHz square wave input signal. Once a voltage is verified across the capacitor, the capacitor must be safely and fully discharged before experimentation proceeds. Following the function test of the CDU, the leads should be disconnected from the primary side of the circuit. The leads connecting the secondary side of the circuit to the capacitor should be shielded in the same manner as in Experiment 1 so that any induced current may be attributed solely to coupling with the transformer.

With the transformer mounted in the breadboard and fixture from Experiment 1, the same process used in Experiment 1 should be repeated, only the peak voltage across the capacitor will be recorded for each shot, rather than magnetic field strength. The sequence of events are very similar, and the experiment should take two people about four hours to complete. Table 1 is a bill of materials for experiments 1 & 2; an experiment protocol and data collection sheet for this experiment follows on subsequent pages.

Table 1: Bill of Materials for Experiments 1 & 2

Part Description	Vendor	Item number	Price	Link	Notes
Vishay surface-mount diode, 600V, 150A	Digikey	VS-150K60A	$ 35.24	http://tiny.sandia.gov/1fgv8	TA-3 might have this equipment
Vishay 1F 25V aluminum electrolytic capacitor	Digikey	MAL210146105E3	$ 269.50	http://tiny.sandia.gov/fjdav	
Vishay/Dale 5kΩ 50W resistor	Digikey	TMC0505K000FE02	$ 36.50	http://tiny.sandia.gov/igkdz	
99.99% Fe Plate, 12" x 12" x 0.08"	American Elements	FE-M-04-PL	$ 812.40	http://tiny.sandia.gov/w26f4	
MuMetal plate, 12" x 12" x 0.08"	Magnetic Shield Corp.	MU080-12-15	$ 287.28	http://tiny.sandia.gov/ioymc	
Zero Gauss Chamber	Magnetic Shield Corp.	ZG-203	$ 1,575.00	http://tiny.sandia.gov/xc4l7	
Inter-8® Weave-Cable, ___'	Magnetic Shield Corp.	MTH-24T	$ 38.00	http://tiny.sandia.gov/bawic	10-foot length
Spira-Shield Flexible Conduit, ____'	Magnetic Shield Corp.	SSC-250	$ 70.20	http://tiny.sandia.gov/9g5uz	10-foot length
		Total	$ 3,124.12		
		Estimated Labor Time	16 hours		

	Action	Initial	Notes
Initial Setup	Connect the transformer to the breadboard so that it is centered on both axes, and insert the breadboard into the slot in the base of the fixture that is sized for this purpose.		
	Solder two sets of leads that will remain secured in a breadboard to the ends of the braided wire, and secure the soldered leads to the holes on the breadboard adjacent to the holes occupied by the transformer pins. Attach the leads connected to the transformer primary to a signal generator, and attach the leads connected to the transformer secondary to the capacitor circuit as shown in Figure 2.		
	Connect a multimeter set to detect DC voltage across the capacitor; test the transformer and capacitor circuit by running a 100kHz, 9V DC square wave through the transformer just long enough for a voltage to appear across the capacitor.		
	Once the transformer/capacitor circuit function has been verified, disconnect the leads on primary side of the transformer.		
	Place the fixture atop E-field absorber, centered under the conductor so that the long axis of the breadboard is aligned with and parallel to the conductor. If the test is performed in an anechoic chamber that prevents reflections of EM energy, disregard this step.		
	Remove the leads from the breadboard, sheathe them within the flexible conduit, and reconnect them to the breadboard.		
	Adjust conductor so that it is 3" above the top surface of the transformer and parallel to the bottom surface of the fixture. Measure and record the actual height.		
	Set up the current source and signal generator; record the current magnitude, voltage, and signal rise time. The target rise time is 10 μs with a decay of 200 μs.		
Unshielded	Ensure that all data is recorded on the attached data sheet for experiment 1.		
	Discharge a single square-wave of current through the conductor; measure and record the peak voltage across the capacitor. Perform three shots total.		
High-purity Fe	Place one 0.125" spacer in each of the four vertical slots on either side of the fixture, and carefully place the high-purity iron plate on the top of the spacers, ensuring adequate space between the top of the transformer and the bottom of the plate.		
	Conduct three shots using the same current and signal characteristics as previous; record the peak voltage across the capacitor for each shot on the datasheet.		
	Remove the plate, replace the 0.125" spacers with the 0.5" spacers, and perform 3 shots. Record each shot.		
	Remove the plate, replace the 0.5" spacers with the 1" spacers, and perform 3 shots. Record each shot.		
μ-metal	Place one 0.125" spacer in each of the four vertical slots on either side of the fixture, and carefully place the μ-metal plate on the top of the spacers, ensuring adequate space between the top of the transformer and the bottom of the plate.		
	Conduct three shots using the same current and signal characteristics as previous; record the peak voltage across the capacitor for each shot on the datasheet.		
	Remove the plate, replace the 0.125" spacers with the 0.5" spacers, and perform 3 shots. Record each shot.		
	Remove the plate, replace the 0.5" spacers with the 1" spacers, and perform 3 shots. Record each shot.		
Zero-Gauss Chamber	Remove the magnetometer and leads from the breadboard and solder the leads directly to the pins of the transformer. Place the transformerer in the fixture, thread the leads through, and assemble the chamber. Slide the conduit up to the opening of the chamber so that it covers as much of the leads as possible. Place the chamber in the cradle, and adjust the conductor so that it is 3" above the center of the chamber.		
	Center the fixture under the conductor, aligned axially.		
	Perform three shots and record each shot on the datasheet.		

Date of Test:

Experiment 2: Magnetic Coupling in a Transformer

Current: Voltage: Rise Time: Conductor Height:	Voltage across Capacitor											
	Unshielded			High-Purity Iron			MuMetal			Zero-Gauss Chamber		
	Shot 1	Shot 2	Shot 3	Shot 1	Shot 2	Shot 3	Shot 1	Shot 2	Shot 3	Shot 1	Shot 2	Shot 3
Spacing 0.125"												
0.5"												
1"												
	Mean									Mean		
Mean 0.125"												
Mean 0.5"												
Mean 1"												
% Reduction 0.125"												
% Reduction 0.5"												
% Reduction 1"												
	Comments/Observations			Comments/Observations			Comments/Observations			Comments/Observations		

Test Engineer _____ Date _____

Facility Engineer _____ Date _____

Safety Engineer _____ Date _____

Manager Consent-to-Test _____ Date _____

4 Breakdown Voltage Testing

Appendix Summary

An assembly process used during a production run of a component led to conductive material being deposited between two disks meant to provide electrical insulation. The component was functionally similar to the rotating switch depicted in Figures 1-4 below; the concern was that if conductive contamination was present between the insulator disks (shown in black), even with the switch in the open position (Figure 4), the switch could allow current through if subjected to high enough voltage: an electric arc could cross the air gap between the conductor in the housing, be conducted via the contaminant to the conductor in the rotating part, and cross to the output conductor in the same fashion.

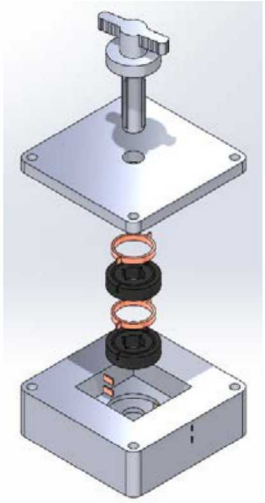

Figure 1: Exploded diagram of switch

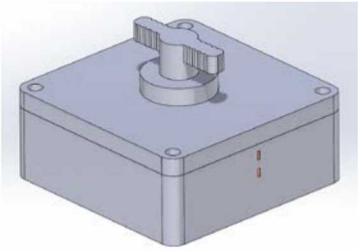

Figure 2: Assembled switch

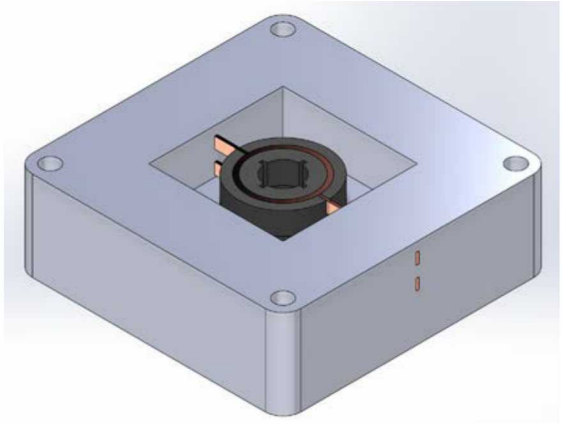

Figure 3: Switch in closed position

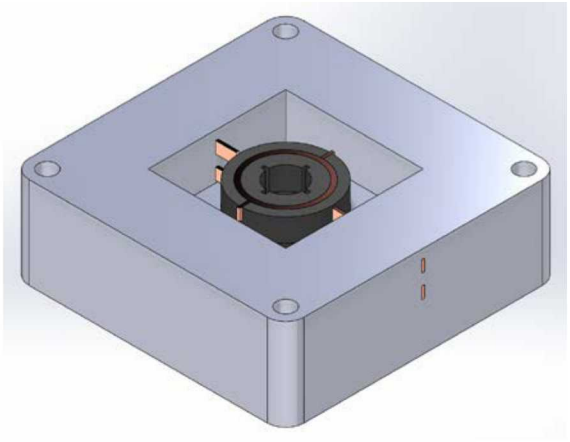

Figure 4: Switch in open position

A series of experiments based on extensive prior testing was conducted to discover what manner of signals could bypass this switch.

5 PMDI Literature Review

Literature Review
Polymethylene Diisocyanate (PMDI) Mechanical, Thermal, Density, and Aging Behavior

Mechanical Properties of Pristine PMDI

There are several types of PMDI foam mentioned in the literature, but the attribute of primary importance for the purposes of examining the mechanical, thermal, and void characteristics is density. The density of a solidified PMDI foam is a function of its chemical composition; the temperature at which it was injected; and whether it was allowed to rise freely, or constrained during the rise process.

Observations at Sandia are that PMDI reaches its glass transition temperature at 150°C, whereupon it softens and its mechanical properties begin to decline with increasing temperature.

Koobor et. al performed a detailed study regarding the mechanical characteristics of PMDI under quasi-static loading. Closed-cell foams deform as a result of the inter-cellular (inter-bubble) wall buckling; with lower-density foams, the intercellular walls are thinner, and therefore buckle under less force, whereas a higher-density foam will have thicker intercellular walls that require more force to effect the same deformation. Once the cells have collapsed, high-density foams develop shear bands along which failure occurs, whereas low-density foams crush without developing shear bands. Under quasi-static loading, the effective plastic Poisson's ratio of a foam is constant, and doesn't reflect the material properties so much as it reflects the cell structure. Once the cells have all collapsed, however, the "true" plastic Poisson's ratio of the material itself emerges. Values of the effective plastic Poisson's ratio for several PMDI foams of differing initial densities can be found on page 25 of [1].

Determining values for the Poisson's ratio under dynamic loading is challenging due mainly to the low wave propagation speed through this type of foam; load cells oriented axially with respect to an impulse have a time delay before dynamic equilibrium is reached, and data is not obtained during this time. Koobor et. al sprayed foam samples with a random pattern of paint and used digital image correlation to relate the foam's physical response to a dynamic input, then calculated the values on page 25 of [1].

Another study by Song et.al used PMDI foams of three different densities, but with cell diameters that were very similar: between 100μm and 200μm. They attempted to overcome the problem of slow wave propagation by using thin samples and carefully tuned impulses through a modified split Hopkinson pressure bar. See pages 22-31 of [2] for stress vs. strain, yield strength vs. strain rate, and yield strength vs. temperature. These plots clearly show where both cell buckling and complete cell compression begin, and indicate that yield strength is proportional to strain rate and inversely proportional to temperature.

Behavior of PMDI in High-Temperature Environments

PMDI subjected to a high-temperature metal surface chars at the contact area, and undergoes solid-to-gas and solid-to-liquid phase transitions; see [3]. The gas advects away from the heat source to regions of foam that are not in direct contact with a heat source, condenses into a liquid phase, and transfers heat to areas of otherwise untouched foam, while the liquid simply erodes further channels in the foam. These liquid channels have different heat transfer characteristics that constitute pathways for accelerated heat transfer to interior portions of foam. Nemer et. al indicate that the high concentration of aniline (a reactive aromatic amine and polyurethane precursor) in the liquid phase could contribute to the formation of channels through chemical interactions with otherwise unaffected foam [4]. In addition, PMDI produces a lot of gas when it decomposes, which can pressurize a container until breach occurs. The chain of events according to Chu et. al starts with the breakdown of polymeric bonds, followed by chemical decomposition into a variety of compounds, and then vaporization of those compounds [5]. Many of the resultant gases are flammable and would ignite in the presence of atmospheric oxygen. The orientation of the foam with respect to a heated surface is important as well, primarily due to the motion of liquefied PMDI. Char on the surface of a foam can act as an insulating barrier that slows decomposition of the material underneath it, but PMDI does not char in such a way that a structure is left behind, as is the case with other foams.

Behavior of PMDI in High-Temperature Environments

The pressure charts on pg. 78 of [3] indicate that a significant gas phase transition begins at about 280°C as evidenced by the sharp increase in pressure. Bilbao et. al report initial decomposition of polyurethane foam into liquid and gas phases in an isothermal environment and nitrogen atmosphere at ~170°C with 10% loss of solid weight at 200°C, up to 30% loss in solid weight at 260°C, and 50% loss at 300°C; all these figures level off at ~2 hours. In an air atmosphere, this changes significantly: 10% solid weight loss at 200°C and 80% loss at 260°C [6]. To explain the difference, Bilbao et. al cite another paper that suggests the presence of oxygen accelerates the rate at which polymeric chains break, while not actually contributing to chemical decomposition. Observations made at Sandia differ, likely owing to different composition: PMDI reaches its glass transition temperature at 150°C, and decomposition begins at 300°C.

Void Characterization

PMDI is usually characterized in terms of density, and some imaging studies have been conducted to study density homogeneity. CT scanning of PMDI foams with a nominal density of 20 lb/ft^3 conducted by Quintana et. al showed actual densities between ~17 lb/ft^3 and ~21.8 lb/ft^3 with a range of void distribution, but doesn't address void formation [7]. This report also shows that foam density is higher at nucleation sites such as walls, which is consistent with diffusing wave spectroscopy and SEM results reported by Roberts et. al [8], addressed below. On a related note, CT scanning of bare PMDI is effective, but would encounter difficulty in an assembled state owing to intervening layers of high-density materials. Quintana et. al mentions that utilizing neutron radiography rather than x-ray radiography is effective at resolving images of low atomic mass materials like polymers behind high atomic mass materials like metals. Neutron radiography is available to a limited extent at TA-V on the SNL NM campus.

Roberts et. al detail the formation of PMDI bubbles in both the "free-rise" and "overpacked" states. Overpacked foam is physically constrained from reaching the minimum density that would be seen in free-rise foam- this is presumably the case for pre-molded foam structures and those that are injected in-situ. Free-rise foam shows less homogeneous bubble size and shape, and experiences shear effects due to friction at nucleation sites that results in oblong bubbles. Overpacking decreases the average bubble size, which commensurately increases the density of the foam and the thickness of intercellular walls, and also increases the uniformity and sphericity of bubbles. Oblong bubbles at nucleation sites become more spherical due to overpacking.

PMDI foams form as the result of two chemical reactions: one which forms CO_2 bubbles, and another that forms the polymer structure. The relative rate of these two reactions determines the density of the resulting foam; a faster CO_2 formation rate relative to the polymerization reaction results in larger bubbles and lower density and vice versa. Observations by Roberts et. al in this context are that larger bubbles tend to form on the top of a free-rise foam, either due to "creaming" – larger bubbles rising to the top of the foam – or due to a slower polymerization reaction leading to lower-viscosity material flowing down the sides of CO_2 bubbles while the CO_2 reaction is still progressing, and that the reaction that forms CO_2 accelerates with increasing temperature. Overpacking mitigates this effect as well; in general, overpacking results in more uniform bubble size and shape throughout a body of foam, with smaller bubbles at nucleation sites. The downside of overpacking, also noticed by Roberts et.al, is that physically constraining a foam while the CO_2 reaction is still ongoing, or accelerating the polymerization reaction relative to the CO_2 reaction and thereby restricting bubble expansion, results in bubble pressures above ambient- which can lead to long-term warpage/shrinkage of the finished part.

Aging

Most accelerated aging tests look at oxidation as the primary degradation mechanism; increasing the temperature of a sample increases the rate of oxidation per the Arrhenius equation, so subjecting samples to elevated temperatures for relatively short periods of time allows for a reasonable extrapolation of their performance after long storage at normal temperatures. One concern in this regard is that if the material is exposed to an oxygen-rich atmosphere but is not initially permeated with oxygen, the surface could suffer accelerated oxidative effects faster than deeper material can be permeated by oxygen. This could result in a gradient of mechanical properties from the surface to the center of a sample, which is not likely representative of an actual aging process at normal temperatures where the atmosphere would have more time to permeate the material.

Aging

However, the PMDI foams in question are blown into sealed containers which contain, at worst, an inert nitrogen atmosphere; the gas contained within the bubbles of the foam itself are primarily CO_2. Concordantly, oxidation shouldn't be much of a concern within these systems.

Some papers indicate that changes in mechanical characteristics increase as the margin between the storage temperature and the material's glass transition temperature narrows, if held at such a temperature for an extended period. This may be explained by molecular mobility not decreasing to zero in the polymer's operational temperature range [9], rather than chemical changes accelerated by temperature- a degradation mechanism that seems to have been neglected in many publications originating at SNL. Regardless, polymers tend to experience an increase in both yield strength and elastic modulus as a result of aging, with the expected decrease in ductility and impact toughness.

References

[1] [SAND2015-0445J] Koobor, B., Mallon, S., Kidane, A., Lu, W. The Deformation and Failure Response of Closed-Cell PMDI Foams Subjected to Dynamic Impact Loading. *Sandia National Laboratories.* 2015. Livermore, CA

[2] [SAND2008-5116J] Song, B., Lu, W., Syn, C., Chen, W. The Effects of Strain Rate, Density and Temperature on the Mechanical Properties of Polymethylene Diisocyanate (PMDI)-Based Rigid Polyurethane Foams during Compression. *Sandia National Laboratories*. 2008. Livermore, CA

[3] [SAND2018-0171] Scott, S. Modeling Heat Transfer and Pressurization of Polymeric Methylene Diisocyanate (PMDI) Polyurethane Foam in a Sealed Container. *Sandia National Laboratories*. 2018. Albuquerque, NM

[4] [SAND2014-18696] Nemer, M., Brooks, C., Shelden, B., Soehnel, M., Barringer, D. Rheological and Mechanical Property Measurements of PMDI foam at Elevated Temperatures. *Sandia National Laboratories.* 2014. Albuquerque, NM

[5] [SAND99-0807C] Chu, T., Hobbs, M., Erickson, K., Ulibarri, T., Renlund, A., Gill, W., Humphries, L., Borek, T. Fire-induced Response in Foam Encapsulants. *Sandia National Laboratories*. 1999. Albuquerque, NM

[6] Bilbao, R., Mastral, J. F., Ceamanos, J., & Aldea, M. E. (n.d.). Kinetics of the thermal decomposition of polyurethane foams in nitrogen and air atmospheres. *Journal of Analytical and Applied Pyrolysis*, *37*(1), 69–82. doi: https://doi.org/10.1016/0165-2370(96)00936-9

[8] [SAND2016-5445] Roberts, C., Mondy, L., Soehnel, G., Brady, C., Shelden, B., Soehnel, M., Garcia, R. Bubble-Size Evolution during Polyurethane Foam Expansion. *Sandia National Laboratories*. 2016. Albuquerque, NM

[9] Struik, L. C. (1977), Physical aging in plastics and other glassy materials. Polym Eng Sci, 17: 165-173. doi:10.1002/pen.760170305